

Provided for non-commercial research and education use.  
Not for reproduction, distribution or commercial use.



This article appeared in a journal published by Elsevier. The attached copy is furnished to the author for internal non-commercial research and education use, including for instruction at the authors institution and sharing with colleagues.

Other uses, including reproduction and distribution, or selling or licensing copies, or posting to personal, institutional or third party websites are prohibited.

In most cases authors are permitted to post their version of the article (e.g. in Word or Tex form) to their personal website or institutional repository. Authors requiring further information regarding Elsevier's archiving and manuscript policies are encouraged to visit:

<http://www.elsevier.com/copyright>



Contents lists available at ScienceDirect

## Journal of Power Sources

journal homepage: [www.elsevier.com/locate/jpowsour](http://www.elsevier.com/locate/jpowsour)

## Review

La-Sr-Ni-Co-O based perovskite-type solid solutions as catalyst precursors in the CO<sub>2</sub> reforming of methaneGustavo Valderrama<sup>a,\*</sup>, Alain Kiennemann<sup>b</sup>, Mireya R. Goldwasser<sup>c</sup><sup>a</sup> Laboratorio de Catálisis, Petróleo y Petroquímica, Unidad de Estudios Básicos, Universidad de Oriente – Núcleo Bolívar, La Sabanita - Calle San Simón, Estado Bolívar 8001, Venezuela<sup>b</sup> Laboratoire des Matériaux et Procédés pour la Catalyse, UMR 7515, ECPM, Université Louis Pasteur, 25 rue Becquerel, 67087 Strasbourg Cedex 2, France<sup>c</sup> Centro de Catálisis, Petróleo y Petroquímica, Facultad de Ciencias – Universidad Central de Venezuela. Paseo los Ilustres, Los Chaguaramos, Caracas 1040, Venezuela

## ARTICLE INFO

## Article history:

Received 25 September 2009

Accepted 1 October 2009

Available online 9 October 2009

## Keywords:

Natural gas

(La-Sr-Ni-Co)-solid solutions

(La-Sr-Ni-Co) perovskite-type oxides

Dry reforming of methane

Carbon deposition

## ABSTRACT

La<sub>1-x</sub>Sr<sub>x</sub>Ni<sub>0.4</sub>Co<sub>0.6</sub>O<sub>3</sub> and La<sub>0.8</sub>Sr<sub>0.2</sub>Ni<sub>1-y</sub>Co<sub>y</sub>O<sub>3</sub> solid solutions with perovskite-type structure were synthesized by the sol-gel resin method and used as catalytic precursors in the dry reforming of methane with CO<sub>2</sub> to syngas, between 873 and 1073 K at atmospheric pressure under continuous flow of reactant gases with CH<sub>4</sub>/CO<sub>2</sub> = 1 ratio. These quaternary oxides were characterized by X-ray diffraction (XRD), BET specific surface area and temperature-programmed reduction (TPR) techniques.

XRD analyses of the more intense diffraction peaks and cell parameter measurements showed formation of La-Sr-Ni-Co-O solid solutions with La<sub>0.9</sub>Sr<sub>0.1</sub>CoO<sub>3</sub> and/or La<sub>0.9</sub>Sr<sub>0.1</sub>NiO<sub>3</sub> as the main crystallographic phases present on the solids depending on the degree of substitution. TPR analyses showed that Sr doping decreases the temperature of reduction via formation of intermediary species producing Ni<sup>0</sup>, Co<sup>0</sup> with particle sizes in the range of nanometers over the SrO and La<sub>2</sub>O<sub>3</sub> phases. These metallic nano particles highly dispersed in the solid matrix are responsible for the high activity shown during the reaction and avoid carbon formation. The presence of Sr in doping quantities also promotes the secondary reactions of carbon formation and water-gas shift in a very small extension during the dry reforming reaction.

© 2009 Elsevier B.V. All rights reserved.

## Contents

1. Introduction .....	1765
2. Experimental .....	1766
2.1. Synthesis of perovskite-type oxides .....	1766
2.2. Characterization .....	1766
2.3. CO <sub>2</sub> reforming of methane .....	1766
3. Results and discussion .....	1766
4. Conclusions .....	1771
Acknowledgements .....	1771
References .....	1771

## 1. Introduction

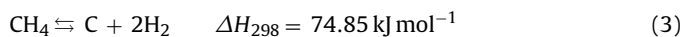
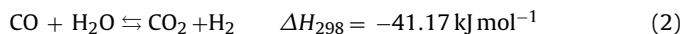
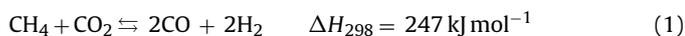
It is well known that the world energy demand is mainly covered by crude oil implying important economic and environmental repercussions, its production centralized in certain regions of the world is subjected to essentially political factors promoting volatility and high prices; moreover, the absence of viable alternatives could be drained the existing reserves in approximately 40 years affecting the global economic development [1]. From an envi-

ronmental point of view, the fossil fuels are the main source of CO<sub>2</sub> emissions main responsible of global heating. This situation requires of new forms of energy sources such as hydrogen which is the more efficient, clean and sure energy considered. These specifications convert natural gas as the excellent raw material for hydrogen production due to their high H/C ratio and it is the energy source that emits less CO<sub>2</sub> by unit of energy produced during its combustion, fulfilling the rigorous environmental specifications imposed at world level [2]. This advantages place natural gas as the first energy source of the planet for the present century. In this sense, new technologies are required to efficiently transform natural gas; among them the CO<sub>2</sub> reforming of methane (Eq. (1)) for the production of synthesis gas (i.e. CO + H<sub>2</sub>), this reaction is typ-

\* Corresponding author. Tel.: +58 285 6329296; fax: +58 285 6321271.

E-mail address: [vgustavo@udo.edu.ve](mailto:vgustavo@udo.edu.ve) (G. Valderrama).

ically influenced by the simultaneous occurrence of the reverse water–gas shift reaction (Eq. (2)) which results in H<sub>2</sub>/CO ratios less than unity, preferable for the synthesis of oxygenated chemicals also because unfavorable CO<sub>2</sub> emissions to the atmosphere are diminished.



One of the major problems is its high thermodynamic potential  $\Delta G^\circ_{298} = 174.6 \text{ kJ mol}^{-1}$ , that implies the use of high temperatures to diminish the free energy (for example  $\Delta G_{1073} = -44.76 \text{ kJ mol}^{-1}$ ) and favor the dry reforming of methane (Eq. (1)), this condition promotes simultaneously the carbon formation (Eq. (3)) especially on the Ni catalysts leading to catalysts deactivation [3]. Therefore, the dry reforming required the use of catalytic systems that inhibit the kinetic of coke formation. The noble metals based catalysts are less sensitive to coking compared to nickel based catalysts. Nevertheless, it is still worthwhile to develop the nickel-based catalysts resistant to the formation of coke because the noble metals are expensive and of limited availability. An alternative is to use Ni and/or Co based precursors with a well-defined structure, as the perovskite-type oxides (ABO<sub>3</sub>) for their interesting redox properties and accessibility, also allows to obtain metallic particles in the order of the nanometers under reducing atmosphere diminishing coke formation and increasing the activity of the catalysts [4].

In previous work we reported the behavior of La<sub>1-x</sub>Sr<sub>x</sub>NiO<sub>3</sub> as catalysts precursors in the dry reforming of methane in a pulse system [5]. The aim of the present work is to investigate the activity and stability of quaternary perovskite-type oxides such as La<sub>1-x</sub>Sr<sub>x</sub>Ni<sub>0.4</sub>Co<sub>0.6</sub>O<sub>3</sub> and La<sub>0.8</sub>Sr<sub>0.2</sub>Ni<sub>1-y</sub>Co<sub>y</sub>O<sub>3</sub> as catalyst precursors in the CO<sub>2</sub> reforming of methane to syngas in a flow system. In addition, the influence of Co in the stability of the LaSrNiO<sub>3</sub> perovskite type oxide and the effect of these solids to avoid coke formation after the reforming reaction was also investigated.

## 2. Experimental

### 2.1. Synthesis of perovskite-type oxides

La<sub>1-x</sub>Sr<sub>x</sub>Ni<sub>0.4</sub>Co<sub>0.6</sub>O<sub>3</sub> and La<sub>0.8</sub>Sr<sub>0.2</sub>Ni<sub>1-y</sub>Co<sub>y</sub>O<sub>3</sub> quaternary oxides were synthesized by the so-called resin method via sol–gel, that consist on the oligomerization of propionate precursors in propionic acid. The expected stoichiometric amounts of acetate salts were separately dissolved in an excess of propionic acid at 415 K. Solutions of metals B (Ni and Co) were mixed and La–Sr solution was then added. The resulting solution was evaporated at a temperature close to the boiling point of the propionic acid until formation of a resin. This resin was dried overnight at 383 K and calcined at 1023 K with an increasing slope of 3 K min<sup>-1</sup> and maintained for 4 h.

### 2.2. Characterization

The solids were characterized before and after catalytic test by X-ray diffraction (XRD), BET specific surface area and temperature-programmed reduction (TPR). XRD analyses were performed on a SIEMENS D5000 diffractometer using a Cu K $\alpha$  radiation. The acquisition of the data depends on the required study; e.g. the scanning of the zone angular from 10° to 90° 2 $\theta$  (step 0.05 2 $\theta$ , time 27 s) be used to obtain the initials phases and cell parameters, and the zone angular between 32° and 35° 2 $\theta$  (step 0.02 2 $\theta$ , time 30 s) be used to confirm the solid solution formation. Phase's recognition was obtained by comparison with JCPDS files using the database PDF and software EVA 3.30 programs.

The specific surface areas were measured by the BET method based on the N<sub>2</sub> physisorption capacity at 77 K, using ~100 mg of sample previously out gassed on Sortometer Coulter SA 3100 equipment.

The TPR studies were carried out in a quartz U-shaped reactor using 50 mg of sample. An H<sub>2</sub> (2 ml min<sup>-1</sup>) diluted in argon (50 ml min<sup>-1</sup>) mixture flows through the reactor heated from room temperature up to 1173 K with a 15 K min<sup>-1</sup> increasing temperature ramp. A thermal conductivity detector (TCD) analysed the effluent gas following passage of a water trap and enabled the quantification of the hydrogen consumption. A calibration of hydrogen was made by injection of a series of pulse (0.5 ml each). The total amount of hydrogen consumption was determined by comparison of the different surfaces. The coke deposition on used catalyst samples was determined by this technique with a similar procedure.

### 2.3. CO<sub>2</sub> reforming of methane

The reaction was performed under continuous flow of reactant gas with CH<sub>4</sub>/CO<sub>2</sub> = 1, over 200 mg of sample without previous reduction, between 873 and 1073 K at atmospheric pressure until completing a “cycle of temperatures”. Two temperature regimes for CO<sub>2</sub> reforming of methane were used, following a similar procedure as reported elsewhere [7], the catalytic parameters were calculated from the equations reported in reference [5].

Catalysts fresh (200 mg) were placed in a 6.6 mm i.d. quartz U-shaped reactor and tested at atmospheric pressure in dry reforming. An CH<sub>4</sub> (5 ml min<sup>-1</sup>) and CO<sub>2</sub> (5 ml min<sup>-1</sup>) mixture flows diluted in Ar (35 ml min<sup>-1</sup>) and N<sub>2</sub> (5 ml min<sup>-1</sup> as internal standard) through the reactor with WHSV = 15 l h<sup>-1</sup> g<sup>-1</sup> and heated under two temperature regimes so-called semi-cycles. The first semi-cycle consists of an increment from room temperature up to 873 K with a rate of 10 K min<sup>-1</sup>; once steady state conditions were reached (~30 min) analyses started and continue within 15 min intervals, followed by an increment of temperature with 50 K intervals from 873 up to 1073 K at 4 K min<sup>-1</sup>. The second semi-cycle consists on the decrease of the temperature from 1073 K up to 873 K a reverse protocol was followed completing a cycle of temperature.

The outlet gas was analysed simultaneously by two gas chromatographs equipped with TCD. The first allows separating hydrogen, nitrogen, methane and monoxide of carbon on a Tami 5 column; the second quantified argon, methane and CO<sub>2</sub> on a Hayesep R column.

## 3. Results and discussion

Results of the different characterizations of the synthesized solids at 1023 K are summarized in the Table 1. It is observed that the resin method via propionic acid favors formation of the perovskite-type structure without the presence of polluting phases (Fig. 1), in the expected stoichiometric with specific surface areas between 6 and 15 m<sup>2</sup> g<sup>-1</sup>, which coincide with our previously reported value [6]. The crystalline phases depends on the extent of substitution for both x and y, the La<sub>0.8</sub>Sr<sub>0.2</sub>Ni<sub>1-y</sub>Co<sub>y</sub>O<sub>3</sub> solids presents for y ≤ 0.4 and for y ≥ 0.6 isomorph structures to La<sub>0.9</sub>Sr<sub>0.1</sub>NiO<sub>3</sub> and La<sub>0.9</sub>Sr<sub>0.1</sub>CoO<sub>3</sub> respectively; while increasing x in the La<sub>1-x</sub>Sr<sub>x</sub>Ni<sub>0.4</sub>Co<sub>0.6</sub>O<sub>3</sub> solids (x ≥ 0.4) favors formation of La<sub>0.6</sub>Sr<sub>0.4</sub>CoO<sub>3</sub> perovskite-type, SrLaCoO<sub>4</sub> spinel-type and NiO mixed oxides structures (Table 1).

A zoom in the zone angular between 32° and 35° (2 $\theta$  scale) corresponding to more intense diffraction peaks of La<sub>1-x</sub>Sr<sub>x</sub>Ni<sub>0.4</sub>Co<sub>0.6</sub>O<sub>3</sub> solids (Fig. 2A), shows a splitting characteristic of rhombohedra symmetry [7,8]. The increment of Sr overlapped both peaks (Fig. 2A) giving rise to an asymmetric wide peak of a distorted rhombohedra, due to formation of a spinel-type structure. While the

**Table 1**  
BET specific surface area and XRD parameters of the synthesized solids at 1023 K.

Precursor solids	SA (m <sup>2</sup> g <sup>-1</sup> )	XRD initial phase <sup>a</sup>	XRD (after)	
			Reduction <sup>b</sup>	Reaction <sup>c</sup>
LaNi <sub>0.4</sub> Co <sub>0.6</sub> O <sub>3</sub>	6	LaCoO <sub>3</sub>	Ni, Co, La(OH) <sub>3</sub>	Ni, Co, La <sub>2</sub> O <sub>2</sub> CO <sub>3</sub>
La <sub>0.9</sub> Sr <sub>0.1</sub> Ni <sub>0.4</sub> Co <sub>0.6</sub> O <sub>3</sub>	11	La <sub>0.9</sub> Sr <sub>0.1</sub> CoO <sub>3</sub>	Ni, Co	
La <sub>0.8</sub> Sr <sub>0.2</sub> Ni <sub>0.4</sub> Co <sub>0.6</sub> O <sub>3</sub>	12	La <sub>0.9</sub> Sr <sub>0.1</sub> CoO <sub>3</sub>	La <sub>2</sub> O <sub>3</sub> , La(OH) <sub>3</sub> SrO	Ni, Co, La <sub>2</sub> O <sub>2</sub> CO <sub>3</sub> , SrO
La <sub>0.6</sub> Sr <sub>0.4</sub> Ni <sub>0.4</sub> Co <sub>0.6</sub> O <sub>3</sub>	9	La <sub>0.6</sub> Sr <sub>0.4</sub> CoO <sub>3</sub> , SrLaCoO <sub>4</sub> , NiO		
La <sub>0.8</sub> Sr <sub>0.2</sub> Ni <sub>0.8</sub> Co <sub>0.2</sub> O <sub>3</sub>	7	La <sub>0.9</sub> Sr <sub>0.1</sub> NiO <sub>3</sub>	Ni, Co, La(OH) <sub>3</sub> SrO	Ni, Co, La <sub>2</sub> O <sub>2</sub> CO <sub>3</sub> , SrO
La <sub>0.8</sub> Sr <sub>0.2</sub> Ni <sub>0.7</sub> Co <sub>0.3</sub> O <sub>3</sub>	15	La <sub>0.9</sub> Sr <sub>0.1</sub> NiO <sub>3</sub>		
La <sub>0.8</sub> Sr <sub>0.2</sub> Ni <sub>0.2</sub> Co <sub>0.8</sub> O <sub>3</sub>	10	La <sub>0.9</sub> Sr <sub>0.1</sub> CoO <sub>3</sub>		

Crystalline phases of the solids: <sup>a</sup>as-synthesized, <sup>b</sup>after reduction (TPR), <sup>c</sup>after the reforming reaction.

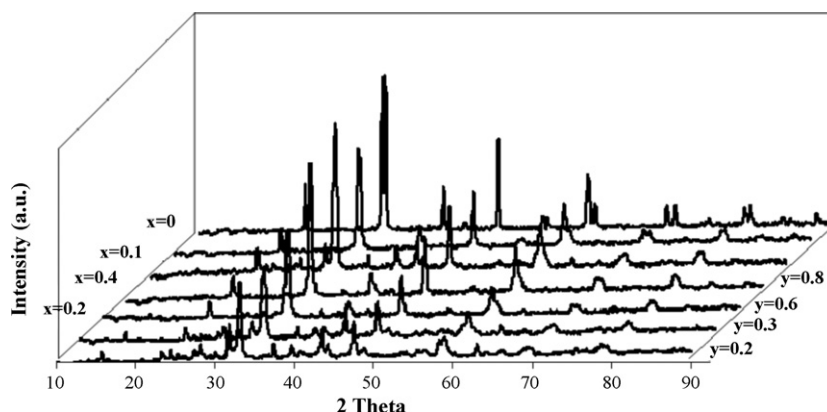


**Fig. 1.** XRD patterns of La<sub>1-x</sub>Sr<sub>x</sub>Ni<sub>0.4</sub>Co<sub>0.6</sub>O<sub>3</sub> and La<sub>0.8</sub>Sr<sub>0.2</sub>Ni<sub>1-y</sub>O<sub>y</sub>O<sub>3</sub> systems.

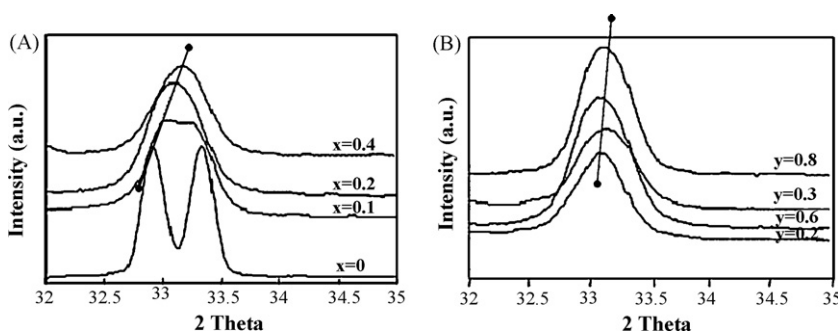


**Fig. 2.** XRD patterns of the more intense peaks of: (A) La<sub>1-x</sub>Sr<sub>x</sub>Ni<sub>0.4</sub>Co<sub>0.6</sub>O<sub>3</sub> and (B) La<sub>0.8</sub>Sr<sub>0.2</sub>Ni<sub>1-y</sub>O<sub>y</sub>O<sub>3</sub>.

La<sub>0.8</sub>Sr<sub>0.2</sub>Ni<sub>1-y</sub>O<sub>y</sub>O<sub>3</sub> quaternary solids (Fig. 2B) did not presented any shift in symmetry in spite of significant variation of Ni and Co content, indicating that Sr (x=0.2) notably influence the second peak of the rhombohedra structure, which is overlapped to an asymmetric wide peak.

Additionally, a linear tendency of the peaks is observed in both series of quaternary solids with the increase of x and/or y (Fig. 2), suggesting the formation of La-Sr-Ni-Co-O solid solution [9], which was confirm by calculating the cell parameters of the crystalline phases (Table 2).

**Table 2**  
Hexagonal and rhombohedra symmetry lattice parameters of synthesized solids.

La <sub>1-x</sub> Sr <sub>x</sub> Ni <sub>0.4</sub> Co <sub>0.6</sub> O <sub>3</sub>	Hexagonal symmetry			Rhomboheda symmetry	
	a (Å)	b (Å)	c (Å)	a (Å)	α
LaNi <sub>0.6</sub> Co <sub>0.4</sub> O <sub>3</sub>	5.4121	5.4121	13.3038	5.4141	59.58
La <sub>0.9</sub> Sr <sub>0.1</sub> Ni <sub>0.4</sub> Co <sub>0.6</sub> O <sub>3</sub>	5.3957	5.3957	13.2801	5.4124	59.78
La <sub>0.8</sub> Sr <sub>0.2</sub> Ni <sub>0.4</sub> Co <sub>0.6</sub> O <sub>3</sub>	5.3960	5.3960	13.2702	5.4104	59.83
La <sub>0.6</sub> Sr <sub>0.4</sub> Ni <sub>0.4</sub> Co <sub>0.6</sub> O <sub>3</sub>	5.3959	5.3959	13.2523	5.4054	59.88
La <sub>0.8</sub> Sr <sub>0.2</sub> Ni <sub>1-y</sub> O <sub>y</sub> O <sub>3</sub>					
La <sub>0.8</sub> Sr <sub>0.2</sub> Ni <sub>0.8</sub> Co <sub>0.2</sub> O <sub>3</sub>	5.4024	5.4024	13.2542	5.4081	59.93
La <sub>0.8</sub> Sr <sub>0.2</sub> Ni <sub>0.7</sub> Co <sub>0.3</sub> O <sub>3</sub>	5.4040	5.4040	13.2535	5.4095	59.97
La <sub>0.8</sub> Sr <sub>0.2</sub> Ni <sub>0.4</sub> Co <sub>0.6</sub> O <sub>3</sub>	5.3961	5.3961	13.2702	5.4104	59.83
La <sub>0.8</sub> Sr <sub>0.2</sub> Ni <sub>0.2</sub> Co <sub>0.8</sub> O <sub>3</sub>	5.4092	5.4092	13.2652	5.4130	59.94

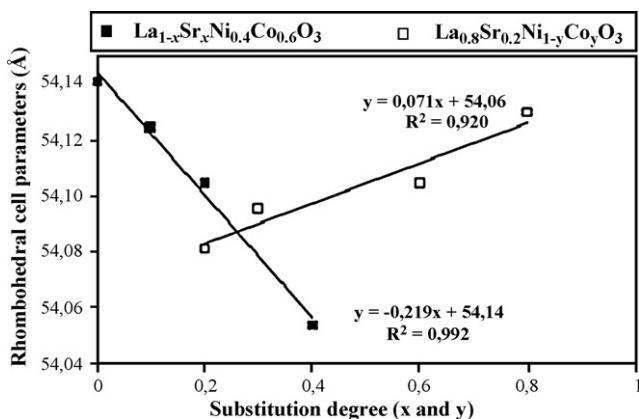


Fig. 3. Rhombohedra cell parameters of  $\text{La}_{1-x}\text{Sr}_x\text{Ni}_{0.4}\text{Co}_{0.6}\text{O}_3$  systems.

To investigate the effect of the partial substitution of A and/or B cations on rhombohedra cell parameters, these were calculated for each x and y value indexing the two most intensive diffraction signals (Fig. 2) in the crystallographic planes (hkl) corresponding to (104) and (024) of  $\text{La}_{0.9}\text{Sr}_{0.1}\text{CoO}_3$  phase (JCPDS 36-1392) to a hexagonal system, since the distorted rhombohedra symmetry is similar to that of an ideal hexagonal symmetry (Table 2). Hexagonal and rhombohedra symmetries were calculated through the equations following:

Hexagonal symmetry:  $a = b \neq c, \alpha = \beta = 90^\circ, \gamma = 120^\circ$

$$\text{Sen}^2\theta = \left(\frac{\lambda^2}{3a^2}\right) \times (h^2 + k^2 + hk) + \left(\frac{\lambda^2 l^2}{4ac^2}\right) \quad (4)$$

$$\frac{l}{4d_{(hkl)}^2} = \left(\frac{1}{3a^2}\right) \times (h^2 + k^2 + hk) + \left(\frac{l^2}{4c^2}\right) \quad (5)$$

Rhomboheda symmetry:  $a = b = c, \alpha = \beta = \gamma \neq 90^\circ$

$$a_R^2 = \left(\frac{a_{\text{HEX}}^2}{3}\right) + \left(\frac{c_{\text{HEX}}^2}{9}\right) \quad (6)$$

$$\text{Sen}\left(\frac{\alpha}{2}\right) = \left(\frac{3}{2\sqrt{3 + (c_{\text{HEX}}/a_{\text{HEX}})^2}}\right) \quad (7)$$

where  $d_{(hkl)}$ , distance between two crystallographic planes (hkl);  $a_R, a_{\text{HEX}}$  and  $c_{\text{HEX}}$ , cell parameters of hexagonal and rhombohedra symmetries, respectively.

Due to the difference in ionic radius, an increase of the cell rhombohedra parameters would be expected when  $\text{La}^{3+}$  (1.36 Å radius) is partially replaced by  $\text{Sr}^{2+}$  (1.44 Å radius) in  $\text{La}_{1-x}\text{Sr}_x\text{Ni}_{0.4}\text{Co}_{0.6}\text{O}_3$ ; however, a lineal decrease was observed with the increase of Sr

(Fig. 3). These tendencies appear to be related to the stability of tetravalent B-site cations, such as stoichiometric formation of  $\text{Co}^{4+}$  (or positive holes) stable in perovskite matrix instead  $\text{Ni}^{4+}$  is not sufficiently stable [10], and formation of lattice oxygen vacancies (Vo), to compensate the charges deficiencies when substituting 3+ by 2+ ions, a mixture of these defects produced as reported by Taroaka et al. [11]. The monotonous increase of  $\text{Sr}^{2+}$  ions promote in a same proportion the  $\text{Co}^{4+}$  formation (0.53 Å high spin radius), which is smaller compared to  $\text{Co}^{3+}$  with 0.61 Å radius and  $\text{Ni}^{3+}$  with 0.60 Å radius (both of high spin) causing a decrease of the distance B–O of the perovskite-type structure reflected in the rhombohedra cell parameters.

On the other hand, the partially substituting of  $\text{Ni}^{3+}$  (0.60 Å radius) by  $\text{Co}^{3+}$  (0.61 Å radius) both of high spin, in  $\text{La}_{0.8}\text{Sr}_{0.2}\text{Ni}_{1-y}\text{Co}_y\text{O}_3$  system, produced a lineal increase of the rhombohedra cell parameters with the cobalt content (Fig. 3), since increase the B–O distance in the perovskite-type structure as previously reported [12]. The substitution of La for Sr ( $x=0.2$ ) also contributes to increase the A–O distance of the perovskite-type structure by the difference of ionic radius, which is reflected in the rhombohedra cell parameters. The previous rhombohedra cell parameters follow Vegart Law [13] that defines solid solutions, that is to say, they show a lineal variation at constant temperature with respect to the degree of substitution x and/or y (Fig. 3), confirming the solid solutions formation among these quaternary systems (La–Sr–Ni–Co).

The TPR profiles of  $\text{La}_{1-x}\text{Sr}_x\text{Ni}_{0.4}\text{Co}_{0.6}\text{O}_3$  and  $\text{La}_{0.8}\text{Sr}_{0.2}\text{Ni}_{1-y}\text{Co}_y\text{O}_3$  (Fig. 4) show that the reduction process starts at lower temperatures when increasing the degree of substitution x and y, due mainly to the presence of Sr that originates unusual oxidation states or positive holes and anionic vacancies, both defects promote the mobility of lattice oxygen to the surface favoring its removal by the reducing gas [14].

Additionally, the TPR profile of these solids (Fig. 4) shows the presence of several peaks, which correspond to different Ni and Co intermediate phases. The splitting of the first peak is due to formation of the spinel-type structure promoted by the presence of Sr [5], which was observed by *ex situ* XRD analyses performed on  $\text{La}_{0.6}\text{Sr}_{0.4}\text{Ni}_{0.4}\text{Co}_{0.6}\text{O}_3$  at different temperatures (Fig. 5), these solid contain a mixture of  $\text{La}_{0.6}\text{Sr}_{0.4}\text{CoO}_3$ ,  $\text{SrLaCoO}_4$  and NiO crystalline phases (Table 1).

The XRD pattern obtained after a TPR until 646 K (first reduction peak, Fig. 5) showed the presence of  $\text{LaSrCoO}_4$  spinel-type phase and small quantities of  $\text{Co}^0$  due to the reduction of  $\text{La}_{0.6}\text{Sr}_{0.4}\text{CoO}_3$ . The second TPR peak appears at 732 K, corresponding to  $\text{Ni}^0$  phase formed by reduction of NiO as observed by XRD (Fig. 5). Finally, a third TPR peak appears at 1013 K, corresponding to  $\text{Co}^0, \text{La}_2\text{O}_3$  and SrO crystalline phases formed by total reduction of  $\text{SrLaCoO}_4$  as observed by XRD (Fig. 5), although the SrO phase was not detected by XRD, its formation cannot be discarded since the determined

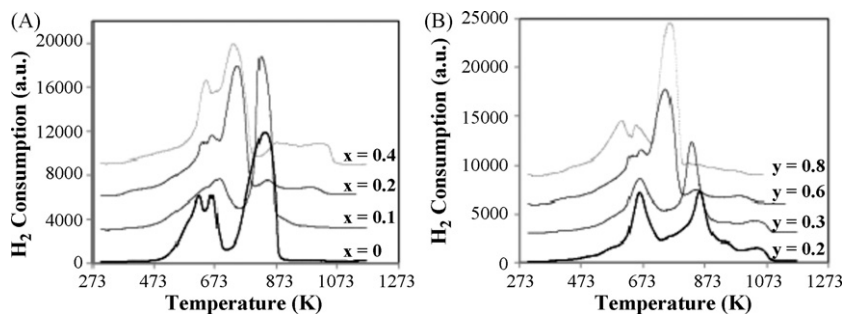
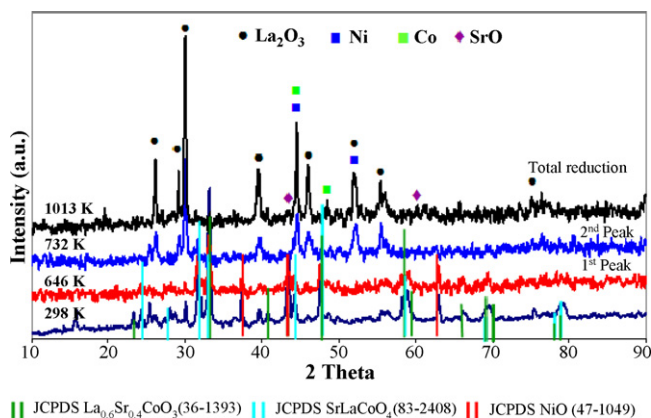


Fig. 4. TPR profiles of: (A)  $\text{La}_{1-x}\text{Sr}_x\text{Ni}_{0.4}\text{Co}_{0.6}\text{O}_3$  and (B)  $\text{La}_{0.8}\text{Sr}_{0.2}\text{Ni}_{1-y}\text{Co}_y\text{O}_3$ .

**Table 3**  
Reduction temperatures, coke percentages and particles size of synthesized solids.

Precursor solids	1st Peak		3rd Peak		3rd Peak		Total		Particle size <sup>c</sup>	
	T (K)	Red (%)	T (K)	Red (%)	T (K)	Red (%)	Red (%)	Coke (%)	Red (nm) <sup>a</sup>	Test (nm) <sup>b</sup>
LaNi <sub>0.4</sub> Co <sub>0.6</sub> O <sub>3</sub>	621	19.8	663	13.4	835	57.3	90.5	0.1	29	29
La <sub>0.9</sub> Sr <sub>0.1</sub> Ni <sub>0.4</sub> Co <sub>0.6</sub> O <sub>3</sub>	623	25.2	835	56.0	–	–	81.2	0.6	38	28
La <sub>0.8</sub> Sr <sub>0.2</sub> Ni <sub>0.4</sub> Co <sub>0.6</sub> O <sub>3</sub>	665	31.1	745	42.0	986	7.9	80.9	2.2	41	40
La <sub>0.6</sub> Sr <sub>0.4</sub> Ni <sub>0.4</sub> Co <sub>0.6</sub> O <sub>3</sub>	644	24.3	673	41.2	1035	15.4	80.9	1.3	42	32
La <sub>0.8</sub> Sr <sub>0.2</sub> Ni <sub>0.8</sub> Co <sub>0.2</sub> O <sub>3</sub>	660	33.7	856	41.5	989	5.6	80.8	1.9	36	33
La <sub>0.8</sub> Sr <sub>0.2</sub> Ni <sub>0.7</sub> Co <sub>0.3</sub> O <sub>3</sub>	660	34.5	830	35.7	1030	9.0	79.2	0.5	32	30
La <sub>0.8</sub> Sr <sub>0.2</sub> Ni <sub>0.2</sub> Co <sub>0.8</sub> O <sub>3</sub>	604	25.3	648	13.0	758	49.6	79.0	1.0	48	30

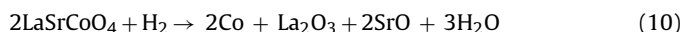
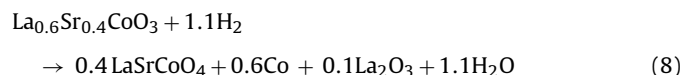
<sup>a</sup>Particles metallic size obtained after of <sup>a</sup>Reduction process, <sup>b</sup>Catalytic reforming.



**Fig. 5.** XRD patterns of La<sub>0.6</sub>Sr<sub>0.4</sub>Ni<sub>0.4</sub>Co<sub>0.6</sub>O<sub>3</sub> after reduction at different temperatures.

particle size was  $\leq 10 \text{ \AA}$ , below the detection limit of X-ray analysis [15].

Based on these results, the reduction steps can be described as follows:



Since the reductions of these solids showed similar profiles (Fig. 4), the La<sub>0.6</sub>Sr<sub>0.4</sub>Ni<sub>0.4</sub>Co<sub>0.6</sub>O<sub>3</sub> observed reduction behavior (Eqs. (8)–(10)) can be extrapolated to all quaternary solids. The decrease of the total reduction percentage with the presence of Sr was always smaller than 100% (Table 3), suggesting a La<sub>1-x</sub>Sr<sub>x</sub>Ni<sub>0.4</sub>Co<sub>0.6</sub>O<sub>3-λ</sub> stoichiometry reduced of the synthesized solids [16].

For La<sub>1-x</sub>Sr<sub>x</sub>Ni<sub>0.4</sub>Co<sub>0.6</sub>O<sub>3</sub>, an increase of the reduction temperature and a considerably decrease of the percentage of reduction was observed as the substitution degree *x* increases (Table 3), indicating that reduction occurs mainly at lower temperatures (except for *x*=0). Assuming that the oxidation states of La, Sr and oxygen are 3+, 2+ and 2– respectively, the observed charge balance indicates a decrease of the formal oxidation state of Ni and/or Co from 3+ (*x*=0) up to 2.6+ (*x*=0.4), since the presence of Sr promotes an electrons doping effect [17]. Similarly, formation of positive holes and vacancies of lattice oxygen when substituting La<sup>3+</sup> for Sr<sup>2+</sup> also promote the mobility of lattice oxygen to the surface [11], both effects favoring the reduction process [14]. Additionally, the La<sub>0.8</sub>Sr<sub>0.2</sub>Ni<sub>1-y</sub>Co<sub>y</sub>O<sub>3</sub> solid solutions showed a similar behavior, where the reduction occurs at lower temperature when *y* increases (Fig. 4) even that both, the host and substitution cations have the same valence. This synergetic effect should be related to the catalytic activity that these precursors may present in the dry reforming of methane [12].

The XRD analyses of the La<sub>1-x</sub>Sr<sub>x</sub>Ni<sub>0.4</sub>Co<sub>0.6</sub>O<sub>3</sub> reduced solids did not show Ni<sup>0</sup>-Co<sup>0</sup> alloy formation and the presence of Sr do not affect notably the metallic particle size calculates by the Scherrer equation [18] showed diameters with value approximately of 41 nm (Table 3), while the increment of Co in La<sub>0.8</sub>Sr<sub>0.2</sub>Ni<sub>1-y</sub>Co<sub>y</sub>O<sub>3</sub> produces a metallic size of particles in the range 32–48 nm. These results suggesting a highly dispersed metallic particles, which play a very important role in the dry reforming of methane avoiding coke formation.

No reduction of La<sub>1-x</sub>Sr<sub>x</sub>Ni<sub>0.4</sub>Co<sub>0.6</sub>O<sub>3</sub> and La<sub>0.8</sub>Sr<sub>0.2</sub>Ni<sub>1-y</sub>Co<sub>y</sub>O<sub>3</sub> precursor's solids was performed prior to catalytic measurements. It was observed that CH<sub>4</sub> and CO<sub>2</sub> conversions measured at different temperatures to that of La<sub>1-x</sub>Sr<sub>x</sub>Ni<sub>0.4</sub>Co<sub>0.6</sub>O<sub>3</sub> did not depend of the substitution degree *x* (Fig. 6), these solids present a similar catalytic behavior to that of LaNi<sub>0.4</sub>Co<sub>0.6</sub>O<sub>3</sub> ternary solid, because the A-site of the perovskite-type structure is inactive for the reaction. Additionally, the observed difference in the conversions during the

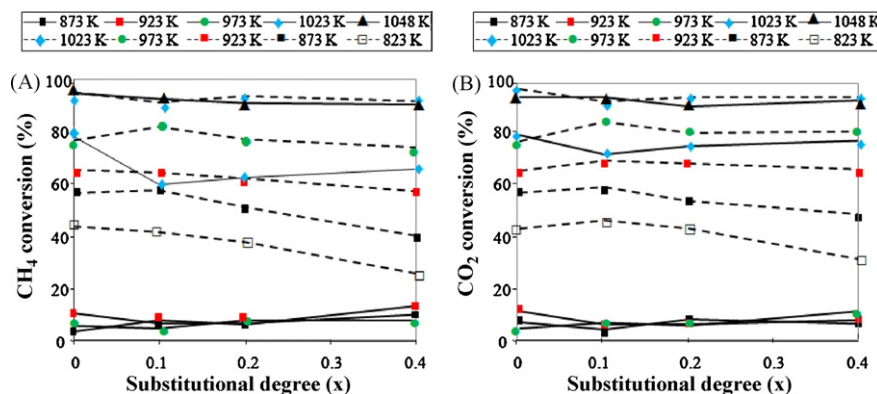


**Fig. 6.** CH<sub>4</sub> (A) and CO<sub>2</sub> (B) conversions on La<sub>1-x</sub>Sr<sub>x</sub>Ni<sub>0.4</sub>Co<sub>0.6</sub>O<sub>3</sub> solid solution as a function of temperature. Rise (—) and descent (---) cycles.

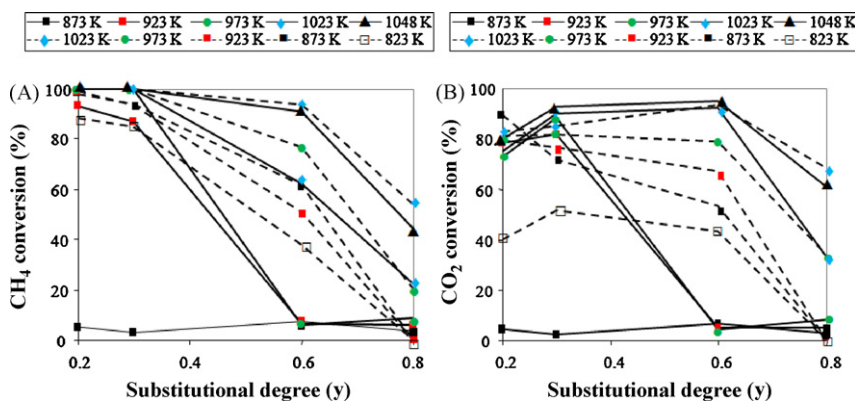


Fig. 7. CH<sub>4</sub> (A) and CO<sub>2</sub> (B) conversions on La<sub>0.8</sub>Sr<sub>0.2</sub>Ni<sub>1-y</sub>Co<sub>y</sub>O<sub>3</sub> solid solution as a function of temperature. Rise (—) and descent (---) cycles.

rise and decrease of the temperature cycle (Fig. 6), known as hysteresis phenomenon [17], is due to the initial lack of activity of the solids at 873 K produced by the absence of active species. Such a phenomenon is not important at higher temperatures ( $T \geq 1073$  K) reaching a stationary state of activation.

It is evident that activation of the solids occurs in situ during the dry reforming, due to the presence of a reducing atmosphere formed by the reaction gases (CH<sub>4</sub>, CO, H<sub>2</sub>) that promotes formation of the active species Ni<sup>0</sup> and Co<sup>0</sup> over La<sub>2</sub>O<sub>3</sub> and SrO (Table 1) according to Eqs. (8)–(10), with metallic particle size in the order on nanometers (Table 3). It is very well-known, that the oxides type perovskite are used as catalytic precursors because they present high metallic dispersion when they undergo reduction.

On the other hand, the La<sub>0.8</sub>Sr<sub>0.2</sub>Ni<sub>1-y</sub>Co<sub>y</sub>O<sub>3</sub> precursor's solids with high Ni contents ( $y \leq 0.3$ ) producing high CH<sub>4</sub> and CO<sub>2</sub> conversions at lower temperatures ( $T \geq 923$  K) (Fig. 7), also these solids solution are activated at lower temperatures in comparison to LaNi<sub>1-y</sub>Co<sub>y</sub>O<sub>3</sub> system [12], which is reflected in the need to use less severe reaction conditions, increasing the useful life time of catalyst and lowering energy consumption.

It was observed that an increase in Co content ( $y \geq 0.6$ ) decreases the catalytic activity (Fig. 7), due to the fact that higher temperatures are required to reduced cobalt to the metallic state according to Eq. (10); increasing the temperature at which the reforming reaction takes place.

Additionally, it was observed that CH<sub>4</sub> conversions are slightly higher than that of CO<sub>2</sub> (Fig. 7), inferring that the secondary reactions of water–gas shift and carbon formation (Eqs. (2) and (3), respectively) is occurring in a very small extension. Accordingly, the methane decomposition reaction (3) increases CH<sub>4</sub> conversion and H<sub>2</sub> selectivity. While water–gas shifts reaction (2) decreases the selectivity to CO and increases H<sub>2</sub> selectivity.

These results indicate that Sr favors those secondary reactions compared to LaNi<sub>0.4</sub>Co<sub>0.6</sub>O<sub>3</sub> solid without Sr doping demonstrated by the small quantities of coke formed (Table 3).

On the other hand, the La<sub>1-x</sub>Sr<sub>x</sub>Ni<sub>0.4</sub>Co<sub>0.6</sub>O<sub>3</sub> solids solution produce similar selectivity's towards CO and H<sub>2</sub>, with a H<sub>2</sub> composition slightly superior to CO indicating that the reactions (2) and (3) occurred in a very small extension, whereas the La<sub>0.8</sub>Sr<sub>0.2</sub>Ni<sub>1-y</sub>Co<sub>y</sub>O<sub>3</sub> system produces selectivity's that depend on the substitution degree y.

This behavior can observe in the CO/H<sub>2</sub> ratio molar obtained for both systems during the catalytic reaction (Fig. 8). For La<sub>1-x</sub>Sr<sub>x</sub>Ni<sub>0.4</sub>Co<sub>0.6</sub>O<sub>3</sub> system the molar ratio is close to 1 suggesting that reaction (Eq. (1)) is favored while for La<sub>0.8</sub>Sr<sub>0.2</sub>Ni<sub>1-y</sub>Co<sub>y</sub>O<sub>3</sub> system this ratio depends on the substitution degree y (Fig. 8) due to the higher Co content which rises the activation temperature of the solid, as previously discussed.

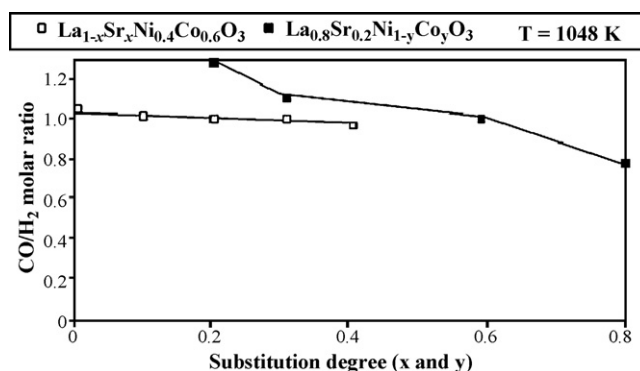


Fig. 8. Reforming of methane; CO/H<sub>2</sub> molar ratio on La<sub>1-x</sub>Sr<sub>x</sub>Ni<sub>0.4</sub>Co<sub>0.6</sub>O<sub>3</sub> systems.

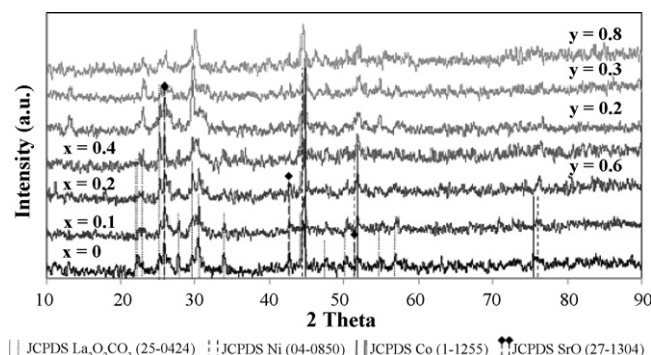
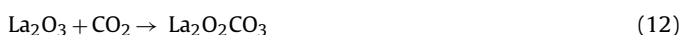


Fig. 9. XRD patterns of after-reaction La<sub>1-x</sub>Sr<sub>x</sub>Ni<sub>0.4</sub>Co<sub>0.6</sub>O<sub>3</sub> and La<sub>0.8</sub>Sr<sub>0.2</sub>Ni<sub>1-y</sub>Co<sub>y</sub>O<sub>3</sub>.

XRD analyses of after-reaction solids reveal the presence of Ni<sup>0</sup>, Co<sup>0</sup>, La<sub>2</sub>O<sub>2</sub>CO<sub>3</sub> and SrO phases (Fig. 9, Table 1) and a decrease the metallic size particles (Table 3); not showing the presence of SrCO<sub>3</sub> phase, although we previously reported that the La<sub>0.6</sub>Sr<sub>0.4</sub>NiO<sub>3</sub> reduced solid produced the SrCO<sub>3</sub> and La<sub>2</sub>O<sub>2</sub>CO<sub>3</sub> phases during the in situ oxidation process under CO<sub>2</sub> atmosphere [5]. In this sense, it could be possible that SrCO<sub>3</sub> phase is formed with a very small particle size which difficult its detection by XRD or it is formed as a reaction intermediary which we propose plays a very important paper in the dry reforming reaction contributing to formation of La<sub>2</sub>O<sub>2</sub>CO<sub>3</sub> and SrO regeneration.

The La<sub>2</sub>O<sub>2</sub>CO<sub>3</sub> phase can be formed according to reactions (11) and (12):



It is important to point out that in spite of the severe reaction conditions used, only small quantities of coke was formed (Table 3), indicating that a high metallic dispersion and a synergistic effect between Ni<sup>0</sup>–Co<sup>0</sup> metallic species occurs which plays a very important role in the catalytic behavior. On the other hand, the incorporation of strontium that produced SrO after-reduction to promote the chemisorptions of CO<sub>2</sub> since presents high affinity for CO<sub>2</sub>, hence La<sub>2</sub>O<sub>2</sub>CO<sub>3</sub> is formed so easily during the dry reforming.

#### 4. Conclusions

The sol–gel method via propionic acid produced highly crystalline quaternary solids of perovskite-type structure with formation of La–Sr–Ni–Co–O solid solution.

Doping quantities of Sr promotes the in situ reduction at lower temperatures producing Ni<sup>0</sup> and Co<sup>0</sup> active species in the order of nanometers highly dispersed on the La<sub>2</sub>O<sub>2</sub>CO<sub>3</sub> and SrO matrix, giving rise to very active catalysts for the dry reforming of methane and inhibiting coke formation in spite of the severe reaction conditions used.

SrCO<sub>3</sub> seems to be an intermediary phase that contributes to formation of the La<sub>2</sub>O<sub>2</sub>CO<sub>3</sub> and SrO regeneration phases that inhibit even more the carbon deposition.

Over La<sub>1–x</sub>Sr<sub>x</sub>Ni<sub>0.4</sub>Co<sub>0.6</sub>O<sub>3</sub> precursors CH<sub>4</sub> and CO<sub>2</sub> conversions are close to the thermodynamic equilibrium conversions at 1023 K and the CO/H<sub>2</sub> molar ratio are close to 1; while on La<sub>1–x</sub>Sr<sub>x</sub>Ni<sub>0.4</sub>Co<sub>0.6</sub>O<sub>3</sub> precursors the conversions decrease and the CO/H<sub>2</sub> molar ratio increases with increasing Co content, due to the fact that an increase in the reduction temperatures favors, in a very small extension, the secondary reactions of carbon formation and water–gas shift.

#### Acknowledgements

The authors are grateful for financial support from the Council of Scientific and Humanistic Development of Venezuelan Central Uni-

versity (UCV-CDCH) and the Draft Law on Science and Technology (LOCTI), through projects PG-03-00-6504-2006 and LOCTI-2008-2009 respectively, To PICS PI 2003000024 and to the Investigation Commission CI-UJO-Bolívar project No. CI-5-010201-1621-09.

#### References

- [1] <http://www.eia.doe.gov/iea/>, January 6, 2009, BP Statistical Review of World Energy, London, 2005.
- [2] M.R. Raupach, G. Marland, P. Ciais, C. Le Quééré, J.G. Canadell, G. Klepper, C.B. Field, Proceedings of the National Academy of Sciences of the United States of America PNAS, 104 (24) (2007) 10288–10293. [www.pnas.org/cgi/doi/10.1073/pnas.0700609104](http://www.pnas.org/cgi/doi/10.1073/pnas.0700609104).
- [3] M.C.J. Bradford, M.A. Vannice, Catal. Rev. 41 (1) (1999) 1–42.
- [4] M.R. Goldwasser, M.E. Rivas, E. Pietri, M.J. Pérez-Zurita, M.L. Cubeiro, A. Grivobal-Constant, G. Leclerq, J. Mol. Catal. A 228 (1–2) (2005) 325–331.
- [5] G. Valderrama, M.R. Goldwasser, C. Urbina de Navarro, J.M. Tatibouët, J. Barrault, C. Batiot-Duperyrat, F. Martínez, Catal. Today 107–108 (2005) 785–791.
- [6] G. Valderrama, M.R. Goldwasser, E. Pietri, M.J. Pérez-Zurita, M.L. Cubeiro, C. Urbina de Navarro, Interciencia 30 (6) (2005) 332–338.
- [7] P. Lacorre, J.B. Torrance, J. Pannetier, A.I. Nasal, P.W. Wang, T.C. Huang, J. Solid State Chem. 91 (2) (1991) 225–237.
- [8] H. Provendier, C. Petit, A. Kiennemann, C. R. Acad. Sci. Paris, IIc Chimie 4 (2001) 57–66.
- [9] J.S. Choi, K.I. Moon, Y.G. Kim, J.S. Lee, C.H. Kim, D. Trimm, Catal. Lett. 52 (1–2) (1998) 43–47.
- [10] N. Yamazoe, Y. Teraoka, Catal. Today 8 (2) (1990) 175–199.
- [11] Y. Teraoka, H.M. Zhang, K. Okamoto, N. Yamazoe, Mater. Res. Bull. 23 (1) (1988) 51–58.
- [12] G. Valderrama, A. Kiennemann, M.R. Goldwasser, Catal. Today 133–135 (2008) 142–148.
- [13] M. Stojanovic, R.G. Haverkamp, C.A. Mims, H. Moudallal, A. Jacobson, J. Catal. 165 (2) (1997) 315–323.
- [14] W.P. Finlandés, Solid State Ionics 129 (1–4) (2000) 145–162.
- [15] G. Giacovazzo, Fundamentals of Crystallography, Oxford University Press, Oxford, RU, 1995, p. 295.
- [16] J.O. Petunchi, E.A. Lombardo, Catal. Today 8 (2) (1990) 201–219.
- [17] M. Medarde, J.Z. Rodríguez-Carvajal, Phys. B: Condens. Mater. 102 (1997) 307–315.
- [18] H.P. Klug, L.E. Alexander, X-Ray Diffraction Procedure for Polycrystalline and Amorphous Materials, 2nd ed., Wiley, New York, 1974.